Nuclear Physics **A528** (1991) 242–252
North-Holland

DYNAMICAL EFFECTS IN HEAVY-ION INTERACTIONS AT BOMBARDING ENERGIES NEAR THE COULOMB BARRIER

A study for the $^{16}O + ^{120}Sn$ system

J. DE BOER, J. FERNÁNDEZ NIELLO, E. HAUBER and E.G. VOGT

Sektion Physik der Universität München, Am Coulombwall 1, D-8046 Garching, Germany

C.H. DASSO

The Niels Bohr Institute, University of Copenhagen, Blegdamsvej 17, DK-2100 Copenhagen Ø, Denmark

M. LOZANO

Departamento de Fisica Atomica, Molecular y Nuclear, Universidad de Sevilla, Apdo. 1065, E-41080 Sevilla, Spain

G. POLLAROLO

Dipartimento de Fisica, Università de Torino and INFN, Torino, Italy

Received 7 November 1990

Abstract: We investigate the magnitude of the effective interactions for elastic and inelastic processes at bombarding energies in the vicinity of the nominal Coulomb barrier. The relevance of higher-order inelastic and transfer processes in defining the strength of the effective couplings is explored in a reaction with a superfluid target, ^{16}O on ^{120}Sn, at center-of-mass energies of 46, 50 and 54 MeV. Significant dynamical effects are found and these appear to be more pronounced in the off-diagonal matrix elements than in the diagonal ones. Theoretical arguments related to the data are presented.

E | NUCLEAR REACTIONS ^{120}Sn (^{16}O, ^{16}O), (^{16}O, $^{16}O'$), $E = 46$, 50, 54 MeV, measured $\sigma(\theta)$, deduced model parameters, dynamical effects role. Optical model.

1. Introduction

Effective interactions are introduced in reaction formalisms to account for the direct transitions between states of a system with a rich structure of intrinsic degrees of freedom. Among various different possibilities we are here interested in the effective couplings designed to incorporate – in terms of a renormalized vertex – higher-order multistep processes. The delays associated with a sequence of such transitions introduce non-localities in time and, as a consequence, the couplings acquire a dynamical content [1]). A characteristic feature of the resulting effective interactions is that they are complex and energy dependent.

In the case of the nucleon–nucleus interaction, for instance, the renormalization of the direct real coupling due to internal modes of excitation in the target gives

rise to the enhancement of the nucleon effective mass observed in the proximity of the Fermi level. Analogous effects involving the interaction of electrons with atomic systems have also been the subject of theoretical and experimental studies (for a general review see e.g. ref. [1]). The wide spread use of imaginary potentials in the analysis of elastic scattering experiments with heavy ions provides yet another example of the practical advantages derived from the introduction of these concepts.

While the need of incorporating into the optical potential an absorptive component has been recognized for a long time it is only recently that attention has been turned to its real counterpart. This contribution to the effective interaction, referred to as the "polarization" correction, combines its effects with that of the static field. Because of this, the presence of the polarization term in most elastic scattering analyses has been masked by a suitable adjustment of the static ion-ion interaction. Detailed studies have, however, unveiled a pronounced energy dependence of the real part of the optical potential at energies close to the Coulomb barrier [2-5]). This behavior is a manifestation of the aforementioned dynamical effects [6]) and correlates with the observed energy dependence of the absorption as the Coulomb threshold is overstepped [7]).

It has been suggested [8]) that similar dynamical effects should be present in the off-diagonal matrix elements, namely those responsible for the excitation of inelastic channels. This expectation also follows from general arguments based on the analytic properties of the couplings [9]). There are important reasons to explore experimentally this class of phenomena. In the elastic channel the nuclear interaction is just strong enough to alter the rate of growth in the ion-ion interaction and to produce the Coulomb barrier. In the case of the inelastic couplings, on the other hand, the nuclear and electric components are better matched. This balance of strengths reflects itself in the presence of a radial node in the corresponding form factors. Inelastic angular distributions are sensitive to the exact position of this cancellation and they therefore provide an accurate tool to extract the relative strength of the electric and nuclear components. Further, as the bombarding energy is lowered below the barrier a convenient energy window opens where the direct transition amplitudes are calculated essentially with Coulomb waves. Thus, the interference patterns in the inelastic cross sections can be studied independently of the optical-model assumptions used to generate the distorted waves.

An interesting point concerns the validity of the collective model for surface vibrations. While this picture is well tested for the real static components of the field [10]), there is no *a priori* reason as to why the macroscopically established connection between the optical potential and the coupling form factors should be preserved when dynamical corrections come into play. In fact, the arguments for relating the absorptive part of the ion potential to the imaginary part of the inelastic form factors are at best qualitative [11]). Moreover, microscopic formalisms for the construction of the effective interactions [12]) reveal that the second-order processes that must implicitly be incorporated in the diagonal matrix elements differ both in

number and in nature from those needed in the off-diagonal matrix elements. Following these arguments it has been speculated [8,12]) that the energy dependence of the inelastic couplings could differ significantly from the ones obtained in the case of the optical potential for elastic scattering. This possibility bears on all structure investigations of nuclear vibrations. It is known, for example, that experiments at different bombarding energies may yield conflicting values for the deformation parameters [see e.g. ref. [13])]. An incorrect assessment of the collective parameters may have important consequences in model interpretations.

This contribution addresses some of these questions in the context of interpreting measurements for elastic scattering and for inelastic excitation of the lowest quadrupole and octupole collective states of ^{120}Sn. Sect. 2 describes the way in which the experiments were performed. In sect. 3 the measured angular distributions are given, together with theoretical calculations that yield the energy dependence of the couplings. A short summary and comments are given in sect. 4.

2. Experimental set-up

The experiments were carried out using beams ($I = 50$–100 particle nA) of ^{16}O provided by the Munich tandem accelerator and using the Q3D magnetic spectrograph. The measurements were performed at three bombarding energies in the center of mass, $E = 54$, 50 and 46 MeV, the last one being approximately the Coulomb barrier for the ^{16}O + ^{120}Sn system. Angular distributions were measured at angles between 65° and 145° in the laboratory system in steps of 10°. At each angle the entire charge-state distribution of the ^{16}O ions was measured, which implied in most cases three runs per angle for the charge states 6^+, 7^+ and 8^+, respectively. At some angles the 5^+ charge state was also measured. The target was isotopically enriched ^{120}Sn (98.4%), 20 μg/cm^2 thick, evaporated onto a 5 μg/cm^2 carbon backing. The reaction products were detected with a position-sensitive ΔE–E ionization chamber in the focal plane of the Q3D spectrograph. The magnetic field of the spectrograph was set in such a way that the ionization chamber accepted an energy range of 92% to 104% of the elastically scattered ^{16}O ions. The normalization for absolute cross sections was obtained by monitoring the Rutherford scattering from the target with a small Bragg chamber placed at 30°.

The data were recorded on magnetic tape in the form of multiparameter events. Each event contained the position and angle of incidence of the particle and the ΔE and E signals. The events recorded by the monitor were scaled down by a factor 10^3. For the calibration of the detector system runs were taken with the Q3D spectrograph placed at 30° and comparing the Rutherford scattering collected in both, the monitor and the Q3D.

Energy spectra of the ^{16}O ions were produced after setting two-dimensional gates in the ΔE–E spectra in order to exclude background events. As an example of the obtained energy resolution, two spectra recorded at center-of-mass angles $\theta = 149.4°$

and 71.9° and $E = 50$ MeV ($q = 8^+$), are shown in fig. 1. At large scattering angles, the elastic peak is well separated from the inelastic ones, which correspond to the excitation of the 2^+ ($E^* = 1.17$ MeV) and 3^- ($E^* = 2.40$ MeV) states in ^{120}Sn. These two states are the only Coulomb excited states in ^{120}Sn as was previously reported in ref. [14]). No other channels have been identified in these measurements. The energy resolution of the spectra for backscattering geometry ($\theta \geq 92.6°$) is mainly due to the energy loss in the target. In the scattering-through geometry ($\theta < 92.6°$) the observed energy resolution is due to straggling and to fluctuations of the energy-loss stemming from the irregular surface of the strongly irradiated target foil. Differential cross sections were extracted from the energy spectra by adding the peak areas of the different charge states weighted by the counts in the monitor detector. The angular distribution for the octupole state in ^{120}Sn was obtained only at the higher bombarding energy, i.e. $E = 54$ MeV.

There are several sources of error contributing to the uncertainty in the cross sections. Among the systematic errors the most important ones are those coming from the absolute normalization based on Rutherford scattering and from the opening angle of the Q3D spectrograph. They were estimated to be about 2%. The

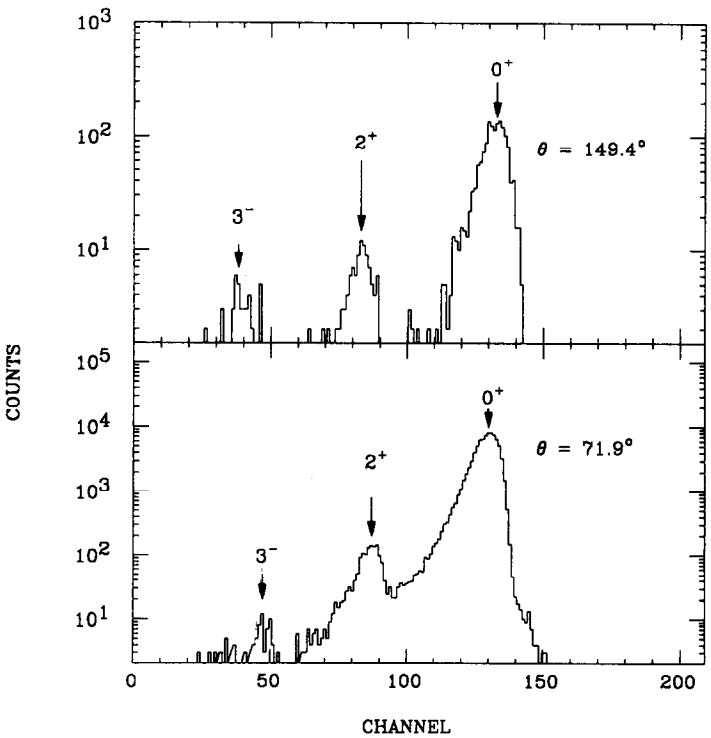

Fig. 1. Energy spectra of the ^{16}O ejectiles from the reaction $^{16}O + ^{120}Sn$ at $E = 50$ MeV. The spectra, corresponding to the 8^+ charge-state, are for the center-of-mass scattering angles $\theta = 149.4°$ (top) and $\theta = 71.9°$ (bottom).

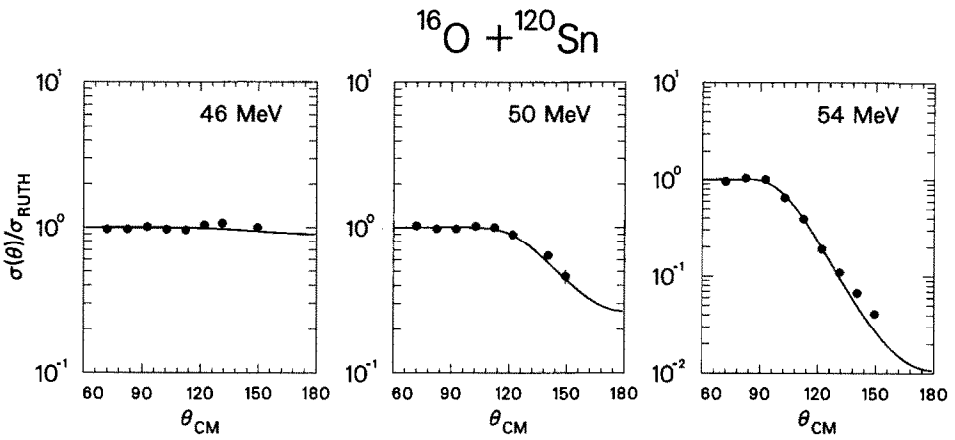

Fig. 2. Angular distributions for elastic events in the reaction $^{16}O+^{120}Sn$ at center-of-mass energies of (a) 46 MeV, (b) 50 MeV and (c) 54 MeV. The solid lines represent the result of calculations performed with the code PTOLEMY using the parameter sets listed in table 1.

error in the cross sections arising from the statistical uncertainty in the peak areas and the unfolding procedure of the elastic and inelastic peaks, particularly at forward angles, ranges from 8% for the elastic to 10–20% for the inelastic data.

3. Extracted data and analysis

A consistent theoretical interpretation of elastic and inelastic processes requires, in principle, a coupled-channel treatment. At the near-barrier energies used in the present experiments the probabilities for inelastic excitation are quite small. Consequently, it is appropriate to analyse the experimental results by DWBA. The pertinent calculations were performed using the code PTOLEMY [15]).

The elastic scattering angular distributions for 46, 50 and 54 MeV center-of-mass energy are collected in fig. 2. The accompanying curves are the results of optical-model calculations using the values of parameters listed in table 1. The magnitude of the extracted potentials

$$U(r, E) = (V(r) + \Delta V(r, E)) + iW(r, E) \quad (1)$$

can be compared for the different bombarding energies by examining the values of

TABLE 1

Optical-model parameters for the reaction $^{16}O+^{120}Sn$ at the indicated bombarding energies

$E_{c.m.}$ (MeV)	V_0 (MeV)	W_0 (MeV)	r_0 (fm)	a_0 (fm)
46	−56.6	−10	1.2	0.64
50	−66	−15	1.2	0.64
54	−57	−30	1.2	0.64

the interaction potential at a fixed radial distance, r_U. The choice of this distance is not very critical for our present purpose since the range of energies covered in the experiments is small compared to the barrier value. The real and imaginary parts of the effective potential are given in the second and third column of table 2. The distance at which the potentials are calculated, $r_U = 11.5$ fm, corresponds approximately to the distance of closest approach. The optical parameters are rather well defined by the data at the two higher bombarding energies but the Rutherford character of the angular distribution obtained for $E = 46$ MeV makes the values for this energy quite uncertain. In particular, the value of $V + \Delta V$ should be regarded only as a lower bound for the real part of the interaction.

In what follows we compare the energy dependence shown by $V + \Delta V$ and W to the results of theoretical predictions. One possibility is to relate the functional dependence of the two quantities by a dispersion relation. On rather general grounds it has been argued [7]) that the polarization and absorptive parts of the optical potential can be related by a dispersion relation of the form

$$\Delta V(E) = \frac{\mathrm{P}}{\pi} \int_{-\infty}^{\infty} \frac{W(E')}{(E' - E)} \mathrm{d}E' , \tag{2}$$

i.e. the one corresponding to the real and imaginary parts of an analytic function. This connection between the functions is taken to hold for any value of the radial coordinate, in particular for $r = r_U$.

In an actual test of the dispersion relations various assumptions can be made regarding the energy dependence of the imaginary part of the optical potential at energies well above the barrier. In particular, when the function is taken to saturate to some constant value or to remain different from zero for $E \to \infty$, the use of a subtracted dispersion relation [1]) becomes necessary. The price paid for an imprecise specification of $W(E)$ over the entire positive real axis is that no control is retained over the absolute value of the polarization correction. It is expected, nevertheless, that the energy dependence of the function ΔV over a narrow range around $E = V_B$ will be well accounted for.

In fig. 3a the three values of $V + \Delta V$ and W listed in table 2 have been plotted as a function of E. The dashed curve included in the frame corresponds to a simple

TABLE 2

Optical potentials and form factors calculated at the distance $r_U = 11.5$ fm. The real, F_R, and imaginary, F_I, parts of the couplings for the lowest 2^+ state of ^{120}Sn are given by the derivatives of a Woods-Saxon function with the same radius and diffuseness parameters as those given in table 1 for the optical potential

$E_{c.m.}$ (MeV)	$V + \Delta V$ (MeV)	W (MeV)	F_R (MeV)	F_I (MeV)
46	−1.02	−0.18	1.57	0.28
50	−1.19	−0.27	1.64	0.63
54	−1.03	−0.54	1.12	0.60

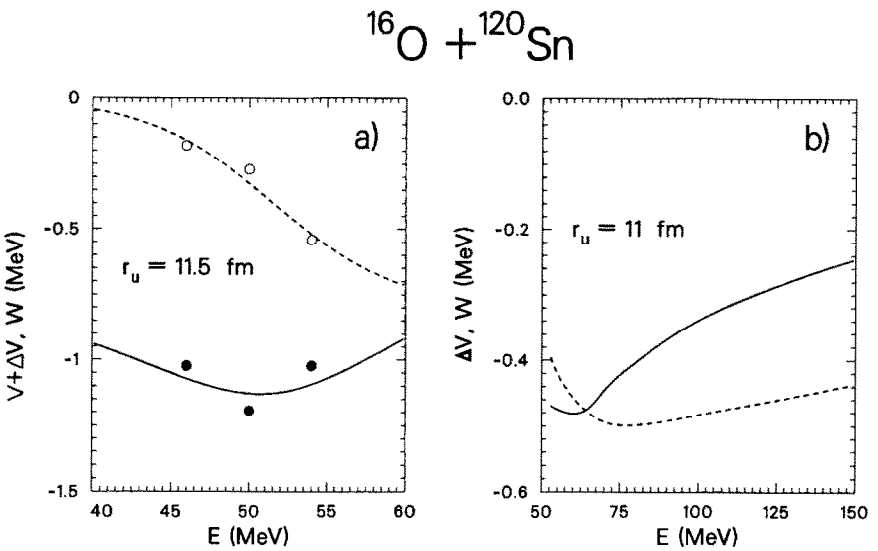

Fig. 3. Energy dependence of the optical potential. (a) The solid circles and open circles indicate, respectively, the values for $V+\Delta V$ and W at $r_U = 11.5$ fm extracted from the data. These are the quantities listed in the second and third column of table 2. The dashed curve included in the frame corresponds to a simple parametrization of the energy dependence of the absorption (see text). The solid curve gives the energy dependence of the effective potential constructed with the dispersion relation (2). Here the value of $V+\Delta V(E)$ has been shifted to be at the level of the experimental points. (b) Energy dependence of the leading correction to the optical potential, ΔV (solid line) and W (dashed line), for a wider range of energies. The values at $r_U = 11$ fm were constructed using the microscopic formalism of ref. [6]).

parametrization of the energy dependence of the absorption as inferred from the data:

$$W(E) = 0.8[1+\exp\tfrac{1}{4}(E-51.5)]^{-1}[1+\exp\tfrac{1}{10}(100-E)]^{-1}, \qquad (3)$$

where both W and E are expressed in MeV. The functional form that was chosen brings the value of W back to zero for large E, thus circumventing the need to use the subtracted version of eq. (2). The energy dependence predicted by the dispersion relation for the total real potential is shown by the solid line, which has been shifted to reach values comparable to those extracted from the experiment. This adjustment is justified because of the inability of the dispersion relation to account for anything more than the functional dependence of ΔV in the narrow energy band in which the data was collected.

In fig. 3b we show the energy dependence of ΔV and W calculated for a broader range of energies, this time generated by the microscopic formalism described in ref. [6]). Although using quite different ways of implementation, the incorporation of dynamical effects in terms of an explicit treatment of particle-transfer channels produces results which are qualitatively similar to the ones obtained from the dispersion relation.

Problems associated with uncertainties in the values of the integrand in eq. (2) do not seem to arise for energies below the barrier, as the absorption is normally taken to go to zero in this limit. The reason invoked for this assumption is that the inelastic channels are no longer open when the reaction cross sections approach their Rutherford values. Microscopic calculations, in their richness of detail, show us otherwise. There is no fundamental change in the energy scales as one lowers the beam energy below the Coulomb barrier. Thus, the adiabatic cut-off functions that control the way in which the different channels are effectively open or closed do not change in any major way. On the other hand, we know that the effective strength of the couplings is not only governed by the energy but also by their radial dependence. Upon examination of the microscopic results it is indeed seen that the presence of the inelastic channels does not affect the elastic process at the lowest energies mostly because of the sharp drop in the strength of the couplings at the relevant distances. This physical aspect is often overlooked when - in standard practice - the dispersion relation is applied at fixed r. In such applications one cannot exclude the possibility that the imaginary component of the couplings is not vanishing sufficiently fast (or at all) at the lower energies. These remarks are not in conflict with any of the successful applications of dispersion relations made so far. In fact, the threshold enhancement of the polarization correction only requires a substantial increase in the absorption as the energy crosses the barrier. Such a gain is predicted by microscopic formulations without resorting to the actual closing of any reaction channels (cf. for instance fig. 3b in the appropriate energy range). Rapid changes with energy within the coupled-channel approach result mostly from the optimum Q-value dependence of particle-transfer processes. These variations are not subject to any particular rule as the transition over the barrier takes place. Contributions from transfer channels may even give rise to polarization corrections that oppose the leading term and thus reduce its effects.

The angular distributions extracted from the experimental data for the lowest 2^+ state in ^{120}Sn are given in fig. 4. The full lines are the results of DWBA calculations performed with inelastic couplings of the magnitude listed in table 2. To achieve a satisfactory fit to the measured cross sections it was necessary to ascribe to the complex inelastic form factors a phase different from the one obtained for the optical potential in the analysis of the elastic data. This confirms the existence of dynamical deviations from the collective macroscopic form of the couplings, i.e. $F = \beta_N R \partial U / \partial r$, and is in agreement with conclusions drawn recently by Smithson *et al.* [16]) from an exhaustive analysis of inelastic cross sections for the lowest 3^- state in ^{208}Pb. From the values of the real and imaginary parts of the coupling listed in table 2, it is difficult to get an idea of the magnitude of the dynamical effects on these off-diagonal terms of the interaction. To facilitate this appreciation let us say that a collective form factor of this strength at the three energies $E = 46$, 50 and 54 MeV corresponds to effective nuclear deformation parameters $\beta_N = 0.17$, $0.21 \exp(i8°)$ and 0.12, respectively. Leaving aside the shift in phase, this amounts to a renormalization

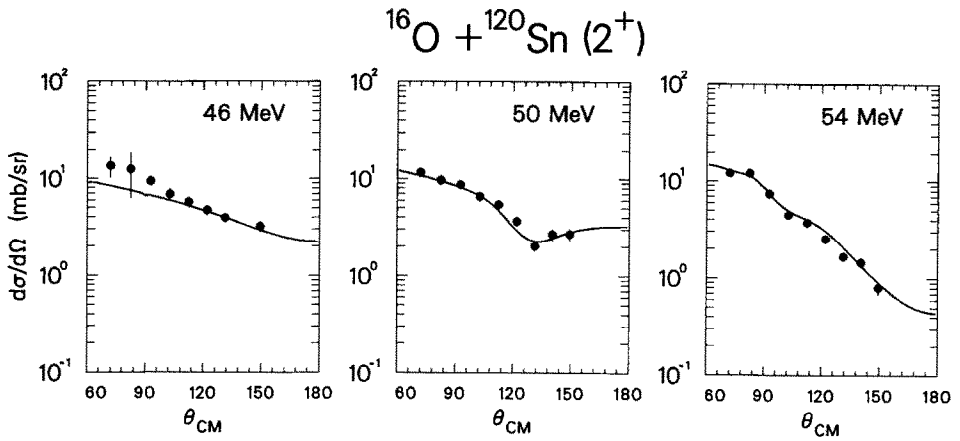

Fig. 4. Angular distributions for the inelastic excitation of the first 2^+ state in ^{120}Sn. The results are from the reaction $^{16}O + ^{120}Sn$ at center-of-mass energies of (a) 46 MeV, (b) 50 MeV and (c) 54 MeV. The solid lines correspond to calculations performed with the code PTOLEMY using the optical potential parameters listed in table 1 and the strength of the couplings given in table 2.

effect of about 80% at the middle energy*, a magnitude considerably larger than the enhancement of the real part of the optical potential at the same bombarding energy. This observation agrees with the earlier analysis of ref. [8]) based on preliminary data by the Daresbury group of Lilley *et al.*

A dispersion relation applied to the data would put in evidence the analytic connection between the real and imaginary components of the off-diagonal part of the couplings [9]). It cannot, however, provide an explanation for the actual magnitude of the observed dynamical effects. A full microscopic construction of the higher-order components of the form factors - though potentially more rewarding - is hard to contemplate in practice as it combines the already large number of intermediate steps for single-particle transitions with the component-rich microscopic wavefunction of the collective vibrational state. Some insight can be extracted from ref. [12]), where the complex calculations were performed for a few single particle-hole configurations. It is seen that as soon as the energy-conservation equation for the second-order process $\alpha \to \gamma \to \beta$, namely

$$\hbar\omega_{\beta\alpha} = \hbar\omega_{\beta\gamma} + \hbar\omega_{\gamma\alpha}$$

is relaxed from the elastic condition $\hbar\omega_{\alpha\alpha} = 0$, a new domain is opened in which the energy of each intermediate transition in a two-step process can be smaller than the Q-value for the leading term. While this feature does not provide a conclusive explanation for the larger strength of the renormalization effects in the off-diagonal couplings it does give an indication as to how second-order transitions may compete - in this case - more efficiently against the direct term.

* Note that the dynamical effects incorporated in the optical potentials given in table 1 would, with this prescription, contribute also to the absolute magnitude of the couplings.

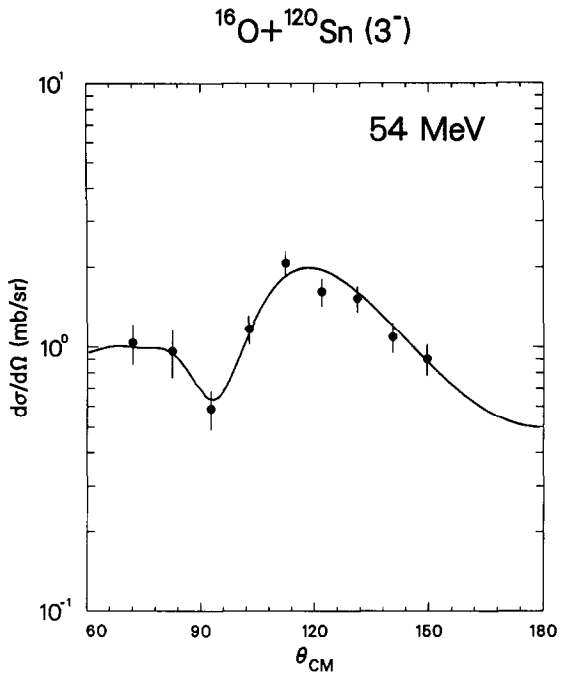

Fig. 5. Angular distributions for the inelastic excitation of the first 3^- state in ^{120}Sn at a center-of-mass energy of 54 MeV. The solid line corresponds to a calculation performed with the PTOLEMY code using the optical potential parameters listed in table 1 and the coupling strength given in the text.

Due to the higher energy resolution and statistics at the highest energy, $E =$ 54 MeV, the area of the lowest octupole state could be determined and the extracted angular distribution is given in fig. 5. The full line shows the fit to the data by a DWBA calculation. The parameters used in this case yield a strength of the couplings at $r = 11.5$ fm of $F_R = 0.63$ MeV and $F_I = 1.10$ MeV. The results of the analysis are interesting because the inferred value of the form factor corresponds to a collective-model fitting with $\beta_C = 0.18$ and $\beta_N = 0.12 \exp(i33°)$. The Coulomb deformation parameter is in good agreement with previous analyses [17]). If the effective value of β_N could be confirmed by further measurements at neighboring bombarding energies this case would provide evidence for the occurrence of negative polarization. This possibility, as stated before, might result from the coupling to transfer-reaction channels.

4. Summary

Angular distributions for elastic and inelastic processes were measured in the reaction $^{16}O+^{120}Sn$ at three bombarding energies. The analysis of the elastic data has allowed to extract values for the optical potential which confirm the presence

of dynamical effects, as previously observed in a variety of systems. The novel results concern the energy dependence of inelastic couplings, represented in this analysis by the form factors for inelastic excitation of the lowest 2^+ state in ^{120}Sn. A large renormalization of the strength of the couplings is inferred, especially for the bombarding energy $E = 50$ MeV, where the balance of strengths of the Coulomb and nuclear components of the couplings is optimal. This balance produces a characteristic pattern in the angular distribution that is very sensitive to the choice of effective nuclear deformation parameters. Although limited to only one energy, the data for the 3^- state is particularly interesting as it suggests the presence of a negative polarization. This unusual possibility calls for further measurements in the tin isotopes for an extended range of energies.

We acknowledge help from N. Gollwitzer, K. Kaiser, A. Lösch and F. Riess during various stages of the experiment. Discussions with G. Madurga and A. Winther are also appreciated. This work was supported by a grant from the Bundesministerium für Forschung and Technologie, Germany (06 LM 171 II) and by the Spanish CICYT project AE90-0932.

References

1) C. Mahaux, P.F. Bortignon, R.A. Broglia and C.H. Dasso, Phys. Rep. **120** (1985) 1
2) A. Baeza, B. Bilwes, R. Bilwes, J. Diaz, J.L. Ferrero, Nucl. Phys. **A419** (1984) 412
3) J.S. Lilley, B.R. Fulton, M.A. Nagarajan, I.J. Thompson and D.W. Banes, Phys. Lett. **B151** (1985) 181
4) B.R. Fulton, D.W. Banes, J.S. Lilley, M.A. Nagarajan and I.J. Thompson, Phys. Lett. **B157** (1985) 250
5) D. Abriola, D. DiGregorio, J.E. Testoni, A. Etchegoyen, M.C. Etchegoyen, J. Fernández Niello, A.M.J. Ferrero, S. Gil, A.O. Macchiavelli, A.J. Pacheco and J. Kittl, Phys. Rev. **C39** (1989) 546
6) C.H. Dasso, S. Landowne, G. Pollarolo and A. Winther, Nucl. Phys. **A459** (1986) 134
7) M.A. Nagarajan, C. Mahaux and G.R. Satchler, Phys. Rev. Lett. **54** (1985) 1136
8) S. Landowne, C.H. Dasso and G. Pollarolo, Phys. Lett. **B178** (1986) 336
9) G.R. Satchler, Nucl. Phys. **A472** (1987) 591
10) R.A. Broglia, C.H. Dasso, G. Pollarolo and A. Winther, Phys. Rep. **48** (1978) 351
11) N. Austern, *Direct nuclear reaction theories* (Wiley, New York, 1970)
12) C.H. Dasso, S. Landowne and G. Pollarolo, Nucl. Phys. **A443** (1985) 365
13) A.M. Bernstein, Adv. Nucl. Phys. **3** (1969) 325
14) N.G. Jonsson, A. Bäcklin, J. Kantele, R. Julin, M. Luontama and A. Passoja, Nucl. Phys. **A371** (1981) 333
15) Computer program PTOLEMY, D.H. Gloeckner, M.H. Macfarlane and S.C. Pieper, Argonne National Laboratory Report No ANL-76-11, 1978, unpublished;
M. Rhoades-Brown, M.H. Macfarlane and S.C. Pieper, Phys. Rev. **21** (1980) 2417; **21** (1980) 2436
16) M.J. Smithson, J.S. Lilley, M.A. Nagarajan, P.V. Drumm, R.A. Cunningham, B.R. Fulton and I.J. Thompson, Nucl. Phys. **A517** (1990) 193
17) R.H. Spear, At. Data Nucl. Data Tables **42** (1989) 55